

# Effects of Ambient Air and Temperature on Ionic Gel Gated Single-Walled Carbon Nanotube Thin-Film Transistor and Circuits

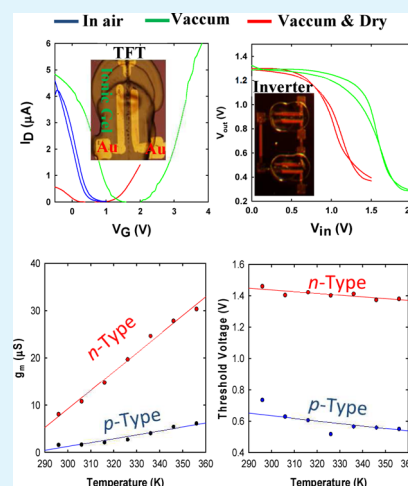
Huaping Li\* and Lili Zhou

Chemelectronics LLC, 440 Hindry Avenue, Unit E, Inglewood, California 90301, United States

## Supporting Information

**ABSTRACT:** Single-walled carbon nanotube thin-film transistor (SWCNT TFT) and circuits were fabricated by fully inkjet printing gold nanoparticles as source/drain electrodes, semiconducting SWCNT thin films as channel materials, PS-PMMA-PS/EMIM TFSI composite gel as gate dielectrics, and PEDOT/PSS as gate electrodes. The ionic gel gated SWCNT TFT shows reversible conversion from *p*-type transistor behavior in air to ambipolar features under vacuum due to reversible oxygen doping in semiconducting SWCNT thin films. The threshold voltages of ionic gel gated SWCNT TFT and inverters are largely shifted to the low value (0.5 V for *p*-region and 1.0 V for *n*-region) by vacuum annealing at 140 °C to exhaustively remove water that is incorporated in the ionic gel as floating gates. The vacuum annealed ionic gel gated SWCNT TFT shows linear temperature dependent transconductances and threshold voltages for both *p*- and *n*-regions. The strong temperature dependent transconductances (0.08  $\mu\text{S}/\text{K}$  for *p*-region, 0.4  $\mu\text{S}/\text{K}$  for *n*-region) indicate their potential application in thermal sensors. In the other hand, the weak temperature dependent threshold voltages ( $-1.5$  mV/K for *p*-region,  $-1.1$  mV/K for *n*-region) reflect their excellent thermal stability.

**KEYWORDS:** printed electronics, semiconducting single-walled carbon nanotubes, ionic gel, thin-film transistor, circuits, threshold voltage, oxygen doping, floating gate



## INTRODUCTION

In comparison to thin-film transistors (TFTs) constructed on low temperature polysilicon,<sup>1</sup> amorphous silicon,<sup>2</sup> metal oxides,<sup>3</sup> and organic materials,<sup>4</sup> single-walled carbon nanotube (SWCNT) TFTs exhibit either equivalent or better figures of merit such as high field effect mobility, low temperature fabrication, good stability, scalability, flexibility, transparency, and low cost (Table 1).<sup>5</sup> In most reports, SWCNT TFTs were gated with oxides such as SiO<sub>2</sub>,<sup>6</sup> Al<sub>2</sub>O<sub>3</sub>,<sup>7</sup> HfO<sub>2</sub>,<sup>8</sup> ZrO<sub>2</sub>,<sup>9</sup> and so on. These SWCNT TFTs showed typical *p*-type behavior in air, and can be converted to ambipolar and even *n*-type behavior under vacuum. Such variable transistor behaviors were also observed in SWCNT TFTs gated with polymer/inorganic salt composites.<sup>10–12</sup> For examples, we found that poly(ethylene oxide) (PEO)/LiClO<sub>4</sub> gated SWCNT TFTs show *p*-type characteristics and polyethylenimine (PEI)/LiClO<sub>4</sub> gated ones display ambipolar features in air. Unfortunately, the reproducibility (yield < 20%) and stability (lifetime < 6 h) of these polymer/inorganic salt gated SWCNT TFTs are poor.<sup>13</sup> Recently, ionic liquid (*N,N*-dimethyl-*N*-(2-methoxyethyl) ammonium bis(trifluoromethanesulfonyl)imide, DEME-TFSI) gated SWCNT TFTs were reported to be *p*-type in air and ambipolar in a nitrogen atmosphere.<sup>14</sup> Similarly, the stable and reproducible ambipolar SWCNT TFTs were obtained under vacuum by employing polymer/ionic liquid composite gels (polystyrene-*b*-poly(methyl methacrylate)-*b*-polystyrene-1-

ethyl-3-methylimidazolium bis(trifluoromethylsulfonyl)imide, PS-PMMA-PS/EMIM-TFSI) as dielectric materials.<sup>15</sup> From literature reports, these convertible traits of SWCNT TFTs originate from either bulk SWCNTs doping or their contacts with electrodes, largely dependent on physical and electric properties of SWCNTs, nature and geometry of electrodes, gate dielectrics, as well as device geometry.<sup>16</sup>

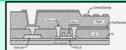
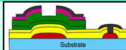
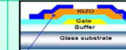


Polymer/ionic liquid composite gels are attracting increasing interests in electronic devices because of their supercapacitance (10  $\mu\text{F}/\text{cm}^2$ ) and carrier accumulation ( $>10^{14}$   $\text{cm}^{-1}$ ).<sup>17–20</sup> These superb properties arise from the generation of 1 nm thick electric double layers (EDL) due to ion motions driven by applied gate potentials.<sup>21</sup> Their capacitances are shown to be independent of gel thickness but exhibit Arrhenius-type temperature dependence in these impedance spectroscopy investigations.<sup>22,23</sup> Polymer/ionic liquid composite gel gated TFTs usually show high transconductance under low operation voltage (within  $\pm 3$  V), good thermal stability ( $<200$  °C), optical transparency, and facile printability.<sup>15,17,18,24–26</sup> The operating mechanism, polarization response time, and stability were extensively investigated for ionic gel gated TFTs.<sup>27–29</sup>

Received: June 26, 2015

Accepted: September 29, 2015

Published: September 29, 2015

Table 1. Comparison of Current TFT Landscape

	LTPS <sup>1</sup>	a-Si <sup>2</sup>	Metal Oxide <sup>3</sup>	Organics <sup>4</sup>	CNT <sup>5</sup>
					
<b>Materials</b>	Polysilicon	Amorphous Si	ZnO based	pentacene	Carbon + polymers dielectric
<b>Mobility</b>	10-100 cm <sup>2</sup> /VS	0.5 cm <sup>2</sup> /VS	1-15 cm <sup>2</sup> /VS	0.1-10 cm <sup>2</sup> /VS	30-100 cm <sup>2</sup> /VS
<b>Uniformity</b>	Poor	Excellent	Good	Good	Good
<b>Stability</b>	Excellent	Poor	Poor	Low	Excellent
<b>Scalable</b>	Limited to <40"	Excellent, >100"	Potential to 100"	Excellent, >100"	Excellent, >100"
<b>Process temperature</b>	High: >400°C	200-300°C	200°C - 350°C	<150°C	<150°C
<b>Cost</b>	High	Low	Medium	Low	Low
<b>Transparent</b>	No	No	No	No	Yes
<b>Flexible</b>	No	No	No	Yes	Yes
<b>Challenges</b>	uniformity, cost, scalability	poor mobility; poor stability	unstable threshold voltage; immature process	poor stability	scalability, all CNT transparent

While the effects of important species in air (oxygen O<sub>2</sub>, and water H<sub>2</sub>O) on ionic gel gated TFTs are not yet addressed.

In this Article, we demonstrate inkjet printing gold nanoparticle electrodes, semiconducting SWCNTs, PS-PMMA-PS/EMIM TFSI composite gel, and poly(3,4-ethylenedioxythiophene)/ poly(styrenesulfonate) (PEDOT/PSS) top electrodes in sequence to form a fully printed ionic gel top-gated SWCNT TFT and circuits on 500 nm SiO<sub>2</sub>/silicon wafers. Their transistor properties were reexamined to display *p*-type and ambipolar behavior in air and under vacuum, respectively. More importantly, the threshold voltages of PS-PMMA-PS/EMIM TFSI top-gated SWCNT TFTs and circuits are remarkably shifted by vacuum annealing, indicative of a significant role played by water molecules inside ionic gels. The temperature dependence of SWCNT TFTs was investigated under vacuum to show linearly increased transconductance and slightly negative threshold voltage shifts for both *p*-type and *n*-type characteristics.

## RESULTS AND DISCUSSION

**Inkjet Printed SWCNT TFT.** The three-dimensional structure of PS-PMMA-PS/EMIM TFSI composite gel gated SWCNT TFTs is shown in Figure 1a, and is fully inkjet printed as follows.

**Stable Gold Electrodes.** The printed silver electrodes become dark after several months.<sup>13</sup> Moreover, the conductivities of these printed silver electrodes are unstable and inconsistent. To circumvent this situation, we surveyed several different commercial inks including platinum, diluted gold nanoparticle inks (50 mg/mL, gold contain), and concentrated gold nanoparticle inks (1 g/mL, gold contain), Cabot and UTDots silver inks. Their curing temperature and performances are compared in Table 2. We remark that the electrodes printed with concentrated gold nanoparticle ink have sheet resistance lower than 1 Ω/□ with uniform surface, excellent adhesion even tolerated for wire bonds, and air stability (no color change in air for several months). All electrodes (150 μm wide) used in this work are inkjet printed from concentrated gold nanoparticle ink (1 g/mL, UTDots) on 500 nm SiO<sub>2</sub>/silicon wafers with a 10 μm tip at a speed of 200 μm/s using a Sonoplot GIX Microplotter II. Printed electrodes were cured at 250 °C for 1 h, and their conductivities were measured before

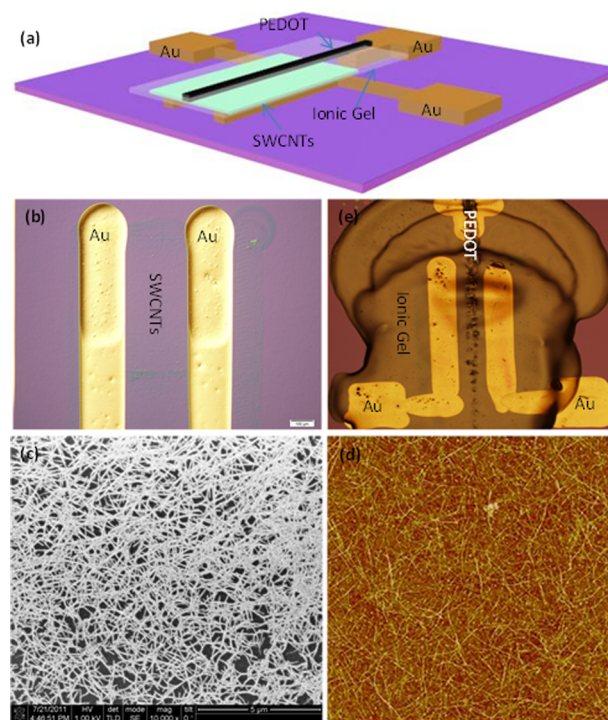


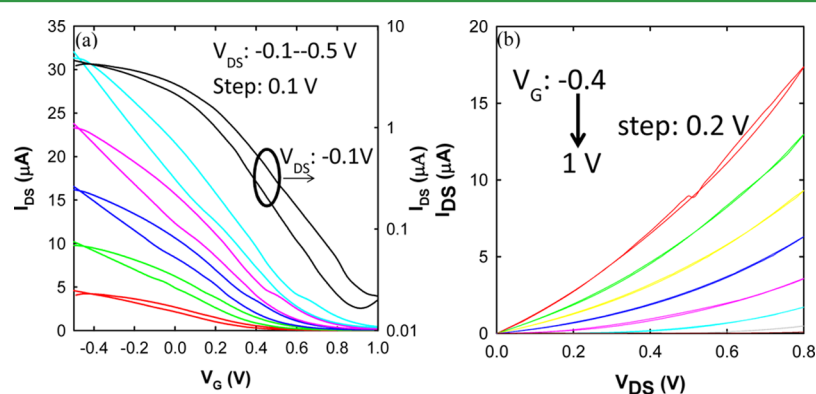
**Figure 1.** (a) Three-dimensional structure of fully printed PS-PMMA-PS/EMIM TFSI composite gel gated SWCNT TFT. (b) Optic microscope image of printed SWCNT film atop of printed gold electrodes. (c) SEM image of printed SWCNT film. (d) AFM image of printed SWCNT film (scale: 5 μm × 5 μm). (e) Optic microscope image of a fully inkjet printed PS-PMMA-PS/EMIM TFSI composite gel gated SWCNT TFT.

use. The designed TFT channel length and width are about  $L_C = 200 \mu\text{m}$  and  $W_C = 1200 \mu\text{m}$ , respectively (seen in Figure 1b).

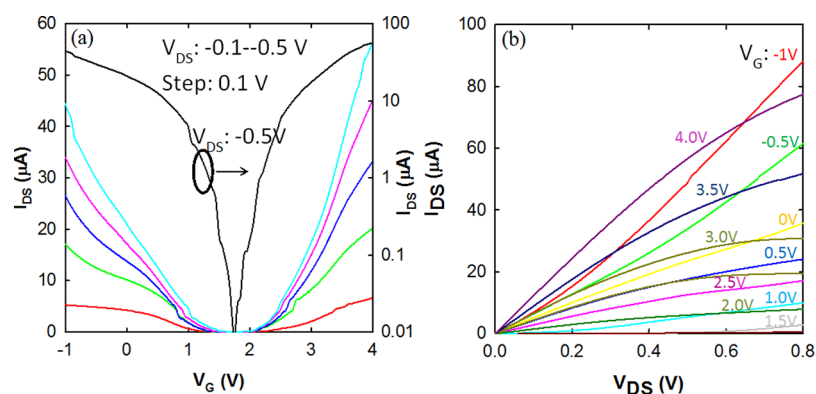
**Semiconducting SWCNT Films.** Semiconducting SWCNTs aqueous solution (0.01 mg/mL, Nano Integrus) was directly inkjet printed with a 30 μm tip at a speed of 80 μm/s on these printed gold electrodes without any pretreatments. The resultant white films were ascribed to enormous chemical dispersants, sodium cholate and sodium dodecylsulfonate, that were used in density gradient ultracentrifugation for SWCNTs separation.<sup>30</sup> After soaking printed semiconducting SWCNTs

Table 2. Comparison of Printed Electrodes

	Platinum	Diluted Gold	Concentrated Gold	Cabot Silver	UTDots Silver
Image					
Sheet Resistance	153.7±37.94 Ω/□	1.55±0.51 Ω/□	0.927±0.545 Ω/□	20.97±10.48 Ω/□	100.60±78.47 Ω/□
Curing Temperature	250°C (30 Min)	300°C (60 Min)	300°C (60 Min)	180°C (20 Min)	120°C (30 Min)
Formulation	Ink (UTDots)	Ink (UTDots)	Ink (UTDots)	Ink (Cabot)	Ink (UTDots)
Uniformity	Good	Good	Excellent	Excellent	Good
Toughness	Good	Good	Good	Poor	Poor
Air Stability	Good	Good	Good	Poor	Poor



**Figure 2.** (a)  $I_{DS}-V_G$  and (b)  $I_{DS}-V_{DS}$  curves of a PS-PMMA-PS/EMIM TFSI composite gel gated SWCNT TFT ( $L_C = 200 \mu\text{m}$  and  $W_C = 1200 \mu\text{m}$ ) by sweeping drain voltage and sweeping gate voltage were characterized on a Keithley 4200 SCS in air.



**Figure 3.** (a)  $I_{DS}-V_G$  and (b)  $I_{DS}-V_{DS}$  curves of a PS-PMMA-PS/EMIM TFSI composite gel gated SWCNT TFT ( $L_C = 200 \mu\text{m}$  and  $W_C = 1200 \mu\text{m}$ ) by sweeping gate voltage and sweeping drain voltage were characterized on a Keithley 4200 SCS under vacuum.

films inside glacial acetic acid for 24 h, uniform and clean semiconducting SWCNTs were obtained and imaged with an optical microscope, a scanning electron microscope (SEM), and an atomic force microscope (AFM) (Figure 1b–d). In this clean process, glacial acetic acid is considered to kinetically neutralize sodium cholate and sodium dodecylsulfonate to form according acids that rapidly diffuse in acetic acids. Clean SWCNT thin films are thus left behind to retain their original position.<sup>31</sup>

**Ionic Gel.** The solution of PS-PMMA-PS (1.5%, weight) and EMIM TFSI (8.5%, weight) in ethyl acetate was prepared.<sup>15</sup> Attempts to inkjet print PS-PMMA-PS/EMIM TFSI solution

using a 30  $\mu\text{m}$  tip lead to rugged composite gels (Supporting Information Figure S1). PS-PMMA-PS/EMIM TFSI ethyl acetate solution was inkjet printed on semiconducting SWCNTs films with wide open tip (inner diameter, 500  $\mu\text{m}$ ) manually to achieve uniform and transparent gels (Figure S1) comparable to those sprayed with Aerosol Jet.<sup>15</sup>

**PEDOT/PSS Top Electrodes.** The aqueous solution of PEDOT/PSS (CLEVIOS VP 4083) cannot be directly inkjet printed on hydrophobic PS-PMMA-PS/EMIM TFSI composite gel. The printable formulation is optimized to be of PEDOT/PSS aqueous solution and isopropyl alcohol (v/v: 1/2) (Supporting Information Table S1), which was manually inkjet



printed on PS-PMMA-PS/EMIM TFSI composite gels using a 10  $\mu\text{m}$  tip. The printed PEDOT/PSS top electrodes on PS-PMMA-PS/EMIM TFSI were baked at 105  $^{\circ}\text{C}$  for 1 h.<sup>15</sup>

With these printing procedures, an ionic gel top-gated SWCNT TFT was fabricated as shown in the optical image (Figure 1e).

**TFT Characterization. In Air.** Ionic gel top-gated SWCNT TFTs were characterized in air with a Keithley 4200 semiconductor characterization system (SCS). The characteristic  $I_{\text{DS}}-V_{\text{G}}$  and  $I_{\text{DS}}-V_{\text{DS}}$  curves of gate-voltage and drain-voltage sweeping are presented in Figure 2, showing typical *p*-type transistor features. By taking the capacitance of 10  $\mu\text{F}/\text{cm}^2$  for PS-PMMA-PS/EMIM TFSI ionic gel, the field-effect hole mobility of composite gel top-gated SWCNT transistors is estimated to be 1.1  $\text{cm}^2/(\text{V s})$  with  $I_{\text{on}}/I_{\text{off}}$  ratio of about 1000, and the threshold voltage at 0.69 V. It is worthy to point out that PS-PMMA-PS/EMIM TFSI top-gated SWCNT TFTs are extremely air stable. The similar  $I-V$  characteristics were obtained from the same device after 6 months. Even after devices were heated at 180  $^{\circ}\text{C}$  in air for 30 min, the properties of devices still remained as is.

**Under Vacuum.** PS-PMMA-PS composite gel top-gated SWCNT TFTs were also characterized under vacuum ( $10^{-6}$  Torr) with a Keithley 4200 SCS. Ambipolar features were observed in  $I_{\text{DS}}-V_{\text{G}}$  and  $I_{\text{DS}}-V_{\text{DS}}$  curves of gate-voltage and drain-voltage sweeping (Figure 3), similar to those in the previous report.<sup>15</sup> The  $I_{\text{on}}/I_{\text{off}}$  ratios of both *n*- and *p*-regions are over 1000. The carrier mobilities of *n*- and *p*-types are 1.2 and 2.0  $\text{cm}^2 \text{V}^{-1} \text{s}^{-1}$  with threshold voltages at 1.3 and 2.3 V, respectively. The relative low carrier mobilities can be ascribed to the long channel length with printed electrodes and low density of SWCNT network in comparison to previous results.<sup>15</sup>

The observed switching transistor properties of composite gel top-gated SWCNT TFTs resemble those of oxides or ionic liquid gated ones.<sup>6-14</sup> When these ionic gel gated SWCNT TFTs were taken out from vacuum chamber and measured in air again, the same *p*-type transistor characteristics were observed. These experimental results indicate that semiconducting SWCNT films covered by PS-PMMA-PS/EMIM TFSI composite gel are facily and reversibly doped by oxygen molecules to suppress *n*-type transistor performances.<sup>32-34</sup> The oxygen doped SWCNT films are further corroborated from their threshold voltage shifts where device measured in air has the lower threshold voltage (0.69 V) than that measured under vacuum (1.3 V) (Figures 2 and 3). However, their mobilities are roughly same possibly due to carrier density induction dominated by EDL<sup>17-29</sup> instead of oxygen doping. These high performances render their applications in logic analogs. The *p*-type transistor properties in air can thus be exploited for low-cost printed electronics such as unipolar *p*-type circuits. While it requires encapsulation and package under vacuum to apply ambipolar behaviors of ionic gel gated SWCNT TFTs for complementary-like circuits.

**Fully Printed Inverter. Characteristics of SWCNT Inverters.** Built on the ambipolar behaviors of ionic gel gated SWCNT TFTs under vacuum; pairs of SWCNT TFTs were connected into complementary-like ionic gel gated SWCNT inverters (Figure 4a). Figure 4b shows the circuit diagram for ionic gel gated SWCNT inverter based on two identical ambipolar ionic gel gated SWCNT TFTs. The PS-PMMA-PS/EMIM TFSI composite gel top-gated SWCNT inverters were characterized on a Keithley 4200 SCS under vacuum. Under a

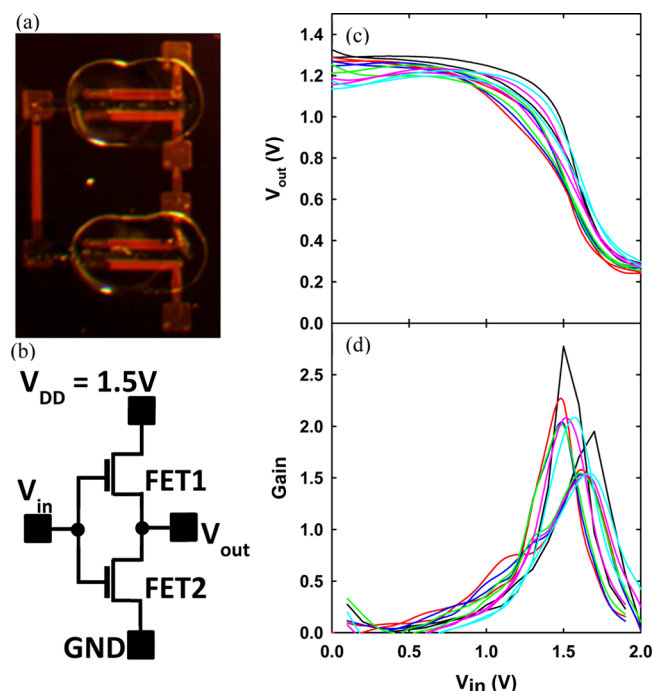


**Figure 4.** (a) Optical microscope image of a PS-PMMA-PS/EMIM TFSI gated SWCNT inverter ( $L_{\text{C}} = 200 \mu\text{m}$  and  $W_{\text{C}} = 1200 \mu\text{m}$ ). (b) Circuit diagram of a complementary-like ionic gel gated SWCNT inverter. (c) Voltage switching curves and (d) voltage gains of a PS-PMMA-PS/EMIM TFSI composite gel gated SWCNT inverter at the temperature varied from 296 to 356 K with steps of 10 K were measured on a Keithley 4200 SCS under vacuum.

voltage supply of  $V_{\text{DD}} = 1.5 \text{ V}$ ,  $V_{\text{out}}$  was detected from 1.3 to 0.3 V when  $V_{\text{in}}$  was swept from 0 to 2 V, showing a rapid voltage switching at  $V_{\text{in}} = 1.5 \text{ V}$  with a voltage gain of 2–3 (Figure 4c and d). Obviously, the detected maximum voltage output ( $V_{\text{out}}^{\text{max}}$ ) is lower than the inverter's threshold voltage. A similar situation was reported in the previous report where SWCNT inverter displayed  $V_{\text{out}}^{\text{max}} = 1.25 \text{ V}$  and  $V_{\text{th}} = 1.2\text{--}1.4 \text{ V}$ .<sup>15</sup> Such types of inverters can not be exploited in high-level digital circuits, such as ring oscillators and decoders, since the output from the previous stage would not enable the switching of the next stage. This abnormality of SWCNT inverters can be ascribed to the inappropriately high threshold voltage ( $V_{\text{th}} > V_{\text{out}}^{\text{max}}$ ) of SWCNT TFTs.<sup>35</sup> Dynamic responses of printed PS-PMMA-PS/EMIM TFSI composite gel top-gated SWCNT Inverters were examined by supplying square-wave inputs (Supporting Information Figure S3). The rise time of inverter is about 0.1  $\mu\text{s}$  and its fall time is 0.05  $\mu\text{s}$ . When the inverter was input with a 100 Hz square wave signal, its output swing reached  $\sim 0.6 \text{ V}$  when  $V_{\text{DD}} = 1 \text{ V}$ . When the input frequency was increased from 100 to 500 Hz, 1 kHz, and 50 kHz, the obtained output swing is reduced from  $\sim 0.6$  to 0.3, 0.3, and 0.16 V, respectively. The inverter looks to function and track best at 50 kHz. The operational stability of the printed PS-PMMA-PS/EMIM TFSI composite gel top-gated SWCNT inverter was tested. After being operated for half a day, no output decrease was detected from the printed PS-PMMA-PS/EMIM TFSI composite gel top-gated SWCNT inverter.

**Thermally Tuning Threshold Voltage.** It is well-known that the threshold voltages of complementary metal oxide semiconductor (CMOS) field effect transistors negatively shift 2 mV when the device temperature is increased by 1 K.<sup>36</sup> PS-PMMA-

PS/EMIM TFSI composite gel top-gated SWCNT inverters were thus characterized under vacuum at varied temperatures from 296 to 356 K with increasing step of 10 K. As seen in Figure 4c, essentially, there is no significant threshold voltage shift observed for SWCNT inverter by raising their temperature up to 60 K. Instead, increasing device temperature slightly decreases voltage gain (Figure 4d). The end threshold voltages of ionic gel gated SWCNT inverter at varied temperatures remain higher than their  $V_{\text{out}}^{\text{max}}$  voltages. These results elicit that the threshold voltage of ionic gel gated SWCNT inverter is nearly temperature independent. Other efforts in using low workfunction source/drain electrodes (silver), tuning charge carriers with dual gate geometry, and doping SWCNT with ammonium hydroxide and polyethylenimine were still unsuccessful to shift the threshold voltage of SWCNT inverter. These failures are also due to the determinant effects of ionic liquid EDL.<sup>17–29</sup>

**Shift Threshold Voltage by Vacuum Annealing.** Further efforts to shift threshold voltages of SWCNT inverters were undertaken by vacuum annealing. After annealing under vacuum at 140 °C for 1 week, PS-PMMA-PS/EMIM TFSI composite gel top-gated SWCNT TFTs and inverters were measured under vacuum with a Keithley 4200 SCS. As shown in Figure 5, their threshold voltages shift down to 0.5 and 1.3 V

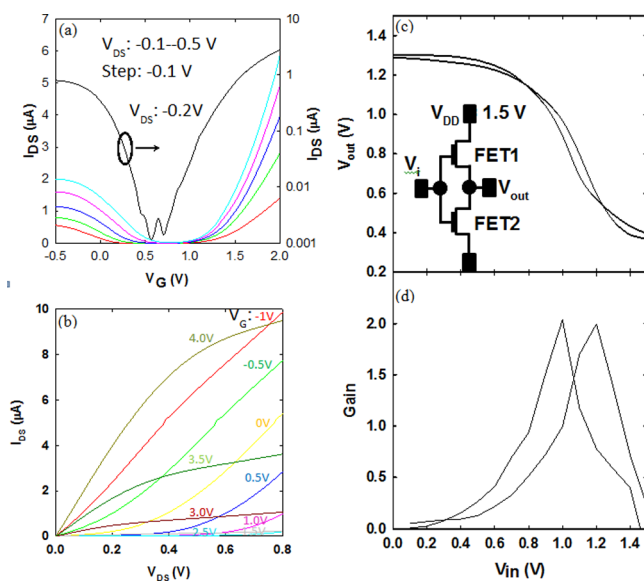


**Figure 5.** (a)  $I_{\text{DS}}-V_{\text{G}}$  and (b)  $I_{\text{DS}}-V_{\text{DS}}$  curves of a vacuum-annealed PS-PMMA-PS/EMIM TFSI composite gel gated SWCNT TFT ( $L_{\text{C}} = 200 \mu\text{m}$  and  $W_{\text{C}} = 1200 \mu\text{m}$ ) by sweeping gate voltage and sweeping drain voltage, (c) voltage switching curve, and (d) voltage gain of a PS-PMMA-PS/EMIM TFSI gated SWCNT inverter under  $V_{\text{DD}} = 1.5$  V were measured on a Keithley 4200 SCS under vacuum.

for  $p$ -region and  $n$ -region, respectively. These results are sharply contrasting those of unannealed ionic gel gated SWCNT TFTs in Figure 4. Though, the observed threshold voltages (especially for  $n$ -type  $V_{\text{th}}$ ) are higher than those in a previous report ( $-0.5$  V for  $n$ -region and  $0.5$  V for  $p$ -region).<sup>15</sup> The resultant switching voltage (1.0 V) of PS-PMMA-PS/EMIM TFSI composite gel top-gated SWCNT inverter is lower than their  $V_{\text{out}}^{\text{max}} = 1.3$  V. Based on this achievement, a three-stage PS-PMMA-PS/EMIM TFSI composite gel top-gated SWCNT ring oscillator was fully printed and exhibited a ring oscillating

frequency of about 400 Hz at a voltage supply of  $V_{\text{DD}} = 1.5$  V (Supporting Information Figure S4).

**Floating Water Gate.** The action executed on PS-PMMA-PS/EMIM TFSI composite gel top-gated SWCNT TFTs and inverters is the removal of water molecules inside ionic gels by exhaustively vacuum annealing. As a result, the on-current of ionic gel gated SWCNT TFTs decreased by an order of magnitude (Figure 5a and b). The on-current is directly related to carrier density induced by gate voltage. Water hydrolysis<sup>37</sup> and oxygen/water couple redox<sup>33</sup> were reported to affect carrier densities of oxide semiconductor ( $V_{\text{G}}: -30$  to  $30$  V) and single-walled carbon tubes ( $V_{\text{G}}: -10$  to  $10$  V), respectively. Especially in these single-walled carbon nanotubes TFTs, the decreased current densities were observed when these TFTs were exposed to water.<sup>33</sup> The low operation gate voltage ( $<4$  V) and increased on-current for these unannealed ionic gel gated SWCNT TFTs lend us to rule out the possibility of the increased carrier densities due to the generation of charged species. Water has been employed as the gate in SWCNT and organic FETs.<sup>38–41</sup> The measured capacitance of water ( $3$ – $20 \mu\text{F}/\text{cm}^2$ )<sup>39</sup> is in the same range as that of PS-PMMA-PS/EMIM TFSI composite gel ( $1$ – $10 \mu\text{F}/\text{cm}^2$ ).<sup>22,23</sup> Thus, the effect of capacitance could also be excluded for the observed threshold voltage shifts. Recently, adsorption of water at the interface usually facilitates charging of semiconductors,<sup>42–46</sup> leading to the increase in current density. Moreover, water also brings about the electrostatic charging of insulators.<sup>47–49</sup> In ionic gel gated SWCNT devices, the EDL of ionic liquid can lead to charge water molecules<sup>50,51</sup> when a bias was applied to the controlled gate (PEDOT/PSS). The charged insulators or charged water thus screen the electric field between gate and SWCNT films, resulting in the shift of SWCNT device's threshold voltage.<sup>52,53</sup>

**Temperature Dependence.** The temperature dependence of PS-PMMA-PS/EMIM TFSI composite gel top-gated CNT TFTs after vacuum annealing were investigated in a vacuum chamber by raising the temperature from 296 to 356 K with steps of 10 K (Figure 6). When the temperature of the device rose up from 296 to 356 K, its current density was increased, and also the turn-on voltage was negatively shifted. By deriving device currents with respect to gate voltage, one can obtain the maximum transconductances ( $g_{\text{m}}^{\text{max}}$ ) at  $V_{\text{DS}} = 0.5$  V. By plotting  $g_{\text{m}}^{\text{max}}$  against varied temperature, one can observe two linear curves, respectively, for  $n$ -type and  $p$ -type transistors. The temperature dependence of  $n$ -type transconductance is  $0.4 \mu\text{S}/\text{K}$  and of  $p$ -type transconductance is  $0.08 \mu\text{S}/\text{K}$ . Such a large temperature effect indicates that printed PS-PMMA-PS/EMIM TFSI composite gel top-gated SWCNT TFTs can be used as *thermal sensors*. By extrapolating the linear portion of the current–voltage of switching gates to off-states, one can extract the threshold voltages ( $V_{\text{th}}$ ) for  $n$ -type and  $p$ -type transistors at different temperatures. By plotting these abstracted threshold voltages against varied temperatures, two linear curves are obtained with slopes of  $1.1$  and  $1.5$  mV/K for  $n$ -type and  $p$ -type behaviors, respectively. The obtained threshold temperature dependences of printed PS-PMMA-PS/EMIM TFSI composite gel top-gated SWCNT TFTs are slightly smaller than that of common complementary metallic oxide semiconductor (CMOS,  $2$  mV/K). This might reflect the better thermal stability of printed PS-PMMA-PS/EMIM TFSI composite gel top-gated SWCNT devices.

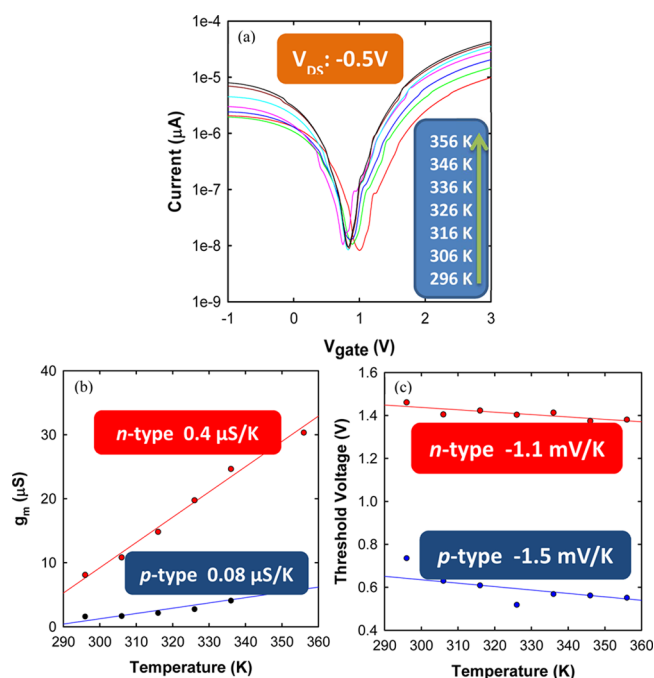


**Figure 6.** (a)  $I_{DS}$ – $V_G$  curves of vacuum-annealed PS-PMMA-PS/EMIM TFSI composite gel gated SWCNT TFT ( $L_C = 200 \mu\text{m}$  and  $W_C = 1200 \mu\text{m}$ ) by sweeping gate voltage at varied temperatures from 296 to 356 K with steps of 10 K were measured on a Keithley 4200 SCS under vacuum ( $10^{-6}$  Torr). Linear curves of peak transconductance ( $g_m$ ) (b) and threshold voltage ( $V_{th}$ ) (c) against the temperature variation were abstracted from  $I_{DS}$ – $V_G$  curves in (a).

## CONCLUSION

Fully inkjet printed SWCNT TFTs and circuits were fabricated with high yield, low cost, and good reproducibility by printing gold nanoparticle ink, semiconducting SWCNTs, PS-PMMA-PS/EMIM TFSI composite gel, and PEDOT/PSS gate electrode in sequence. Ionic gel gated SWCNT TFT and circuits are air stable and tolerate temperature as high as  $<200^\circ\text{C}$ . The reversible conversion between  $p$ -type (in air) and ambipolar (under vacuum) transistor features can be plausibly interpreted as the reversible oxygen doping in semiconducting SWCNTs to suppress  $n$ -type transistor behavior of SWCNT TFTs. The maximum transconductance ( $g_m^{\text{max}}$ ) and  $V_{th}$  of vacuum annealed ionic gel gated SWCNT TFTs respond linearly to the temperature variation. The field effect mobilities of ionic gel gated SWCNT TFTs are in the range from 1 to  $2 \text{ cm}^2/(\text{V s})$ , and their  $I_{on}/I_{off}$  ratios are over 1000. Complementary-like ionic gel gated SWCNT inverters exhibit voltage switching at 1.5 V with a gain of about 2, a rise time of  $0.1 \mu\text{s}$ , and a fall time of  $0.05 \mu\text{s}$ , and functioned/tracked best at 50 kHz when a power supply of  $V_{DD} = 1.5 \text{ V}$  was applied under vacuum. The performances (transistor features,  $V_{th}$ , transconductances) of PS-PMMA-PS/EMIM TFSI composite gel gated SWCNT TFT and circuits are largely affected by oxygen, water, and temperature variation. Therefore, the effects of oxygen, water, and temperature should be carefully considered in these emerging electronic devices gated with ionic gels.<sup>17–20</sup>

## ASSOCIATED CONTENT

### Supporting Information

The Supporting Information is available free of charge on the ACS Publications website at DOI: 10.1021/acsami.5b05727.

Experimental details, formulations of PEDOT/PSS solution, optimal inkjet printed ionic gel, dynamic response of ionic gel gated SWCNT inverter, and oscillating frequency of a three-stage ionic gel gated SWCNT ring oscillator (PDF)

## AUTHOR INFORMATION

### Corresponding Author

\*E-mail: lihuaping.li@gmail.com.

### Notes

The authors declare no competing financial interest.

## ACKNOWLEDGMENTS

We thank Professor K. Wang and Dr. J. Tang of Department of Electrical Engineering at University of California Los Angeles for comments and technical assistance.

## REFERENCES

- Uchikoga, S. Low-Temperature Polycrystalline Silicon Thin-Film Transistor Technologies for System-on-Glass Displays. *MRS Bull.* **2002**, *27*, 881–886.
- Snell, A. J.; Mackenzie, K. D.; Spear, W. E.; LeComber, P. G.; Hughes, A. J. Application of Amorphous Silicon Field Effect Transistors in Addressable Liquid Crystal Display Panels. *Appl. Phys.* **1981**, *24*, 357–362.
- Kamiya, T.; Hosono, H. *NPG Asia Mater.* **2010**, *2*, 15–22. Park, J. S.; Maeng, W.-J.; Kim, H.-S.; Park, J.-S. Review of Recent Developments in Amorphous Oxide Semiconductor Thin-Film Transistor Devices. *Thin Solid Films* **2012**, *520*, 1679–1693.
- Forrest, S. R. The Path to Ubiquitous and Low-Cost Organic Electronic Appliances on Plastic. *Nature* **2004**, *428*, 911–918.
- Sun, D.-M.; Timmermans, M. Y.; Tian, Y.; Nasibulin, A. G.; Kauppinen, E. I.; Kishimoto, S.; Mizutani, T.; Ohno, Y. Flexible High-Performance Carbon Nanotube Integrated Circuits. *Nat. Nanotechnol.* **2011**, *6*, 156–161.
- Tans, S. J.; Verschueren, A. R. M.; Dekker, C. Room-Temperature Transistor Based on a Single Carbon Nanotube. *Nature* **1998**, *393*, 49–52.
- Bachtold, A.; Hadley, P.; Nakanishi, T.; Dekker, C. Logic Circuits with Carbon Nanotube Transistors. *Science* **2001**, *294*, 1317–1320.
- Javey, A.; Tu, R.; Farmer, D. B.; Guo, J.; Gordon, R. G.; Dai, H. High Performance n-Type Carbon Nanotube Field-Effect Transistors with Chemically Doped Contacts. *Nano Lett.* **2005**, *5*, 345–348.
- Javey, A.; Kim, H.; Brink, M.; Wang, Q.; Ural, A.; Guo, J.; McIntyre, P.; McEuen, P.; Lundstrom, M.; Dai, H. High- $\kappa$  Dielectrics for Advanced Carbon-Nanotube Transistors and Logic Gates. *Nat. Mater.* **2002**, *1*, 241–246.
- Lu, C. G.; Fu, Q.; Huang, S. M.; Liu, J. Polymer Electrolyte-Gated Carbon Nanotube Field-Effect Transistor. *Nano Lett.* **2004**, *4*, 623–627.
- Zhou, Y. X.; Gaur, A.; Hur, S.-H.; Kocbas, C.; Meitl, M. A.; Shim, M.; Rogers, J. A. p-Channel, n-Channel Thin Film Transistors and p-n Diodes Based on Single Wall Carbon Nanotube Networks. *Nano Lett.* **2004**, *4*, 2031–2035.
- Ozel, T.; Gaur, A.; Rogers, J. A.; Shim, M. Polymer Electrolyte Gating of Carbon Nanotube Network Transistors. *Nano Lett.* **2005**, *5*, 905–911.
- Chen, P. C.; Fu, Y.; Aminirad, R.; Wang, C.; Zhang, J. L.; Wang, K. L.; Galatsis, K.; Zhou, C. W. Fully Printed Separated Carbon Nanotube Thin Film Transistor Circuits and Its Application in Organic Light Emitting Diode Control. *Nano Lett.* **2011**, *11*, 5301–5308.
- Okimoto, H.; Takenobu, T.; Yanagi, K.; Miyata, Y.; Shimotani, H.; Kataura, H.; Iwasa, Y. Tunable Carbon Nanotube Thin-Film Transistors Produced Exclusively via Inkjet Printing. *Adv. Mater.* **2010**, *22*, 3981–3986.



- (15) Ha, M. J.; Xia, Y.; Green, A. A.; Zhang, W.; Renn, M. J.; Kim, C. H.; Hersam, M. C.; Frisbie, C. D. Printed, Sub-3V Digital Circuits on Plastic from Aqueous Carbon Nanotube Inks. *ACS Nano* **2010**, *4*, 4388–4395.
- (16) Avouris, P.; Chen, J. Nanotube Electronics and Optoelectronics. *Mater. Today* **2006**, *9*, 46–54.
- (17) Cho, J. H.; Lee, J. Y.; Xia, Y.; Kim, B. S.; He, Y. Y.; Renn, M. J.; Lodge, T. P.; Frisbie, C. D. Printable Ion-Gel Gate Dielectrics for Low-Voltage Polymer Thin-Film Transistors on Plastic. *Nat. Mater.* **2008**, *7*, 900–906.
- (18) Xia, Y.; Zhang, W.; Ha, M. J.; Cho, J. H.; Renn, M. J.; Kim, C. H.; Frisbie, C. D. Printed Sub-2 V Gel-Electrolyte-Gated Polymer Transistors and Circuits. *Adv. Funct. Mater.* **2010**, *20*, 587–594.
- (19) Chen, C.-F.; Park, C.-H.; Boudouris, B. W.; Horng, J.; Geng, B. S.; Girit, C.; Zettl, A.; Crommie, M. F.; Segalman, R. A.; Louie, S. G.; Wang, F. Controlling Inelastic Light Scattering Quantum Pathways in Graphene. *Nature* **2011**, *471*, 617–620.
- (20) Lee, M. Y.; Williams, J. R.; Zhang, S. P.; Frisbie, C. D.; Goldhaber-Gordon, D. Electrolyte Gate-Controlled Kondo Effect in SrTiO<sub>3</sub>. *Phys. Rev. Lett.* **2011**, *107*, 256601.
- (21) Ono, S.; Miwa, K.; Seki, S.; Takeya, J. A Comparative Study of Organic Single-Crystal Transistors Gated with Various Ionic-Liquid Electrolytes. *Appl. Phys. Lett.* **2009**, *94*, 063301.
- (22) Lee, K. H.; Zhang, S. P.; Lodge, T. P.; Frisbie, C. D. Electrical Impedance of Spin-Coated Ion Gel Films. *J. Phys. Chem. B* **2011**, *115*, 3315–3321.
- (23) Zhang, S. P.; Lee, K. H.; Frisbie, C. D.; Lodge, T. P. Ionic Conductivity, Capacitance, and Viscoelastic Properties of Block Copolymer-Based Ion Gels. *Macromolecules* **2011**, *44*, 940–949.
- (24) Vaillancourt, J.; Zhang, H. Y.; Vasinajindakaw, P.; Xia, H. T.; Lu, X. J.; Han, X. L.; Janzen, D. C.; Shih, W.-S.; Jones, C. S.; Stroder, M.; Chen, M. Y. H.; Subbaraman, H.; Chen, R. T.; Berger, U.; Renn, M. All Ink-Jet-Printed Carbon Nanotube Thin-Film Transistor on a Polyimide Substrate with an Ultrahigh Operating Frequency of over 5 GHz. *Appl. Phys. Lett.* **2008**, *93*, 243301.
- (25) Kim, J. K.; Jang, H.; Lee, S. K.; Hong, B. H.; Ahn, J.-H.; Cho, J. H. High-Performance Flexible Graphene Field Effect Transistors with Ion Gel Gate Dielectors with Ion Gel Gate Dielectrics. *Nano Lett.* **2010**, *10*, 3464–3466.
- (26) Lee, S.-K.; Kim, B. J.; Jang, H.; Yoon, S. C.; Lee, C. J.; Hong, B. H.; Rogers, J. A.; Cho, J. H.; Ahn, J.-H. Strachable Graphene Transistors with Printed Dielectrics and Gate Electrodes. *Nano Lett.* **2011**, *11*, 4642–4646.
- (27) Lee, J. Y.; Panzer, M. J.; He, Y. Y.; Lodge, T. P.; Frisbie, C. D. Ion Gel Gated Polymer Thin-Film Transistors. *J. Am. Chem. Soc.* **2007**, *129*, 4532–4533.
- (28) Cho, J. H.; Lee, J. Y.; He, Y. Y.; Kim, B. S.; Lodge, T. P.; Frisbie, C. D. High-Capacitance Ion Gel Gate Dielectrics with Faster Polarization Response Times for Organic Thin Film Transistors. *Adv. Mater.* **2008**, *20*, 686–690.
- (29) Lee, J. Y.; Kaake, L. G.; Cho, J. H.; Zhu, X.-Y.; Lodge, T. P.; Frisbie, C. D. Ion gel-gated Polymer Thin-Film Transistors: Operating Mechanism and Characterization of Gated Dielectric Capacitance, Switching Speed, and Stability. *J. Phys. Chem. C* **2009**, *113*, 8972–8981.
- (30) Arnold, M. S.; Green, A. A.; Hulvat, J. F.; Stupp, S. I.; Hersam, M. C. Sorting Carbon Nanotubes by Electronic Structure Using Density Differentiation. *Nat. Nanotechnol.* **2006**, *1*, 60–65.
- (31) Li, H. P.; Zhou, H. Visualizing Surfactants Helically Wrapped Semiconducting Single-Walled Carbon Nanotubes and Their Impacts on Electronic Properties (submitted).
- (32) Collins, P. G.; Bradley, K.; Ishigami, M.; Zettl, A. Extreme Oxygen Sensitivity of Electronic Properties of Carbon Nanotubes. *Science* **2000**, *287*, 1801–1804.
- (33) Nouchi, R.; Tomita, H.; Ogura, A.; Kataura, H.; Shiraishi, M. Logic Circuits Using Solution-Processed Single-Walled Carbon Nanotube Transistors. *Appl. Phys. Lett.* **2008**, *92*, 253507.
- (34) Aguirre, C. M.; Levesque, P. L.; Paillet, M.; Lapointe, F.; St-Antoine, B. C.; Desjardins, P.; Martel, R. The Role of the Oxygen/Water Redox Couple in Suppressing Electron Conduction in Field-Effect Transistors. *Adv. Mater.* **2009**, *21*, 3087–3091.
- (35) Kergoat, L.; Herlogsson, L.; Piro, B.; Pham, M. C.; Horowitz, G.; Crispin, X.; Berggren, M. Tuning the Threshold Voltage in Electrolyte-Gated Organic Field-Effect Transistors. *Proc. Natl. Acad. Sci. U. S. A.* **2012**, *109*, 8394–8399.
- (36) Weste, N. H. E.; Eshrahan, K. *Principles of CMOS VLSI Design*, 2nd ed.; Addison Wesley: Boston, 1994.
- (37) Ohta, H.; Sato, Y.; Kato, T.; Kim, S. W.; Nomura, K.; Ikuhara, Y.; Hosono, H. Field-Induced Water Electrolysis Switches an Oxide Semiconductor from an Insulator to a Metal. *Nat. Commun.* **2010**, *1*, 118.
- (38) Rosenblatt, S.; Yaish, Y.; Park, J. W.; Sazonova, V.; McEuen, P. L. High Performance Electrolyte Gated Carbon Nanotube Transistors. *Nano Lett.* **2002**, *2*, 869–872.
- (39) Kergoat, L.; Herlogsson, L.; Braga, D.; Piro, B.; Pham, M.-C.; Crispin, X.; Berggren, M.; Horowitz, G. A Water-Gate Organic Field-Effect Transistor. *Adv. Mater.* **2010**, *22*, 2565–2569.
- (40) Duan, X. J.; Gao, R. X.; Xie, P.; Cohen-Karni, T.; Qing, Q.; Choe, H. S.; Tian, B. Z.; Jiang, X. C.; Lieber, C. M. Intracellular Recordings of Action Potentials by an Extracellular Nanoscale Field-Effect Transistor. *Nat. Nanotechnol.* **2012**, *7*, 174–179.
- (41) Kergoat, L.; Battaglini, N.; Miozzo, L.; Piro, B.; Pham, M.-C.; Yassar, A.; Horowitz, G. Use of Poly(3-Hexylthiophene)/Poly(Methyl Methacrylate) (P3HT/PMMA) Blends to Improve the Performance of Water-Gated Organic Field-Effect Transistors. *Org. Electron.* **2011**, *12*, 1253–1257.
- (42) Park, Y. M.; Salleo, A. Dual-Gate Organic Thin Film Transistors as Chemical Sensors. *Appl. Phys. Lett.* **2009**, *95*, 133307.
- (43) Shim, J. H.; Lui, C. H.; Ko, T. Y.; Yu, Y.-J.; Kim, P.; Heinz, T. F.; Ryu, S. Water-Gated Charge Doping of Graphene Induced by Mica Substrates. *Nano Lett.* **2012**, *12*, 648–654.
- (44) Cramer, T.; Steinbrecher, T.; Koslowski, T.; Case, D. A.; Biscarni, F.; Zerbetto, F. Water-Induced Polaron Formation at the Pentacene Surface: Quantum Mechanical Molecular Mechanics Simulations. *Phys. Rev. B: Condens. Matter Mater. Phys.* **2009**, *79*, 155316.
- (45) McCarty, L. S.; Whitesides, G. M. Electrostatic Charging Due to Separation of Ions at Interfaces: Contact Electrification of Ionic Electrets. *Angew. Chem., Int. Ed.* **2008**, *47*, 2188–2207.
- (46) McCarty, L. S.; Winkleman, A.; Whitesides, G. M. Ionic Electrets: Electrostatic Charging of Surfaces by Transferring Mobile Ions upon Contact. *J. Am. Chem. Soc.* **2007**, *129*, 4075–4088.
- (47) Schein, L. B. Recent Progress and Continuing Puzzles in Electrostatics. *Science* **2007**, *316*, 1572–1573.
- (48) Gouveia, R. F.; Galebeck, F. Electrostatic Charging of Hydrophilic Particles due to Water Adsorption. *J. Am. Chem. Soc.* **2009**, *131*, 11381–11386.
- (49) Jacobs, H. O.; Whitesides, G. M. Submicrometer Patterning of Charge in Thin-Film Electrets. *Science* **2001**, *291*, 1763–1766.
- (50) Ovchinnikova, K.; Pollack, G. H. Can Water store Charge? *Langmuir* **2009**, *25*, 542–547.
- (51) Santos, L. P.; Ducati, T. R. D.; Balestrin, L. B. S.; Galebeck, F. Water with Excess Electric Charge. *J. Phys. Chem. C* **2011**, *115*, 11226–11232.
- (52) Yu, W. J.; Kang, B. R.; Lee, I. H.; Min, Y.-S.; Lee, Y. H. Majority Carrier Type Conversion with Floating Gates in Carbon Nanotube Transistors. *Adv. Mater.* **2009**, *21*, 4821–4824.
- (53) Sekitani, T.; Yokota, T.; Zschieschang, U.; Klauk, H.; Bauer, S.; Takeuchi, K.; Takamiya, M.; Sakurai, T.; Someya, T. Organic Nonvolatile Memory Transistors for Flexible Sensor Arrays. *Science* **2009**, *326*, 1516–1519.